Materials Science & Engineering A 693 (2017) 1–13

Contents lists available at ScienceDirect

Materials Science & Engineering A

journal homepage: www.elsevier.com/locate/msea

Origin of unusual fracture in stirred zone for friction stir welded 2198-T8 Al-Li alloy joints

Y. Tao[a,b], D.R. Ni[a,*], B.L. Xiao[a], Z.Y. Ma[a], W. Wu[c], R.X. Zhang[c], Y.S. Zeng[c,**]

[a] Shenyang National Laboratory for Materials Science, Institute of Metal Research, Chinese Academy of Sciences, Shenyang 110016, China
[b] University of Chinese Academy of Sciences, Beijing 100049, China
[c] AVIC Beijing Aeronautical Manufacturing Technology Research Institute, Beijing 100024, China

ARTICLE INFO

Keywords:
Friction stir welding
Aluminum-Lithium alloys
Microstructure
Fracture behavior

ABSTRACT

Friction stir welded (FSW) joints of conventional precipitation-hardened aluminum alloys usually fracture in the lowest hardness zone (LHZ) during tension testing. However, all of the FSW joints of a 2198-T8 Al-Li alloy fractured in the stirred zone (SZ) instead of the LHZ with the welding parameters of 800 rpm-200 mm/min and 1600 rpm-200 mm/min under the condition that no welding defects existed in the SZ. The experiment results revealed that lazy S was not the dominant factor resulting in the unusual fracture. The SZ consisted of three subzones, i.e., the shoulder-affected zone, the pin-affected zone, and the transition zone between them. While the former two zones were characterized by fine and equiaxed recrystallized grains, incompletely dynamically recrystallized microstructure containing coarse elongated non-recrystallized grains was observed in the transition zone. The transition zone exhibited the lowest average Taylor factor in the SZ, resulting in a region that was crystallographically weak. Furthermore, obvious lithium segregation at grain boundaries was observed in the transition zone via time-of-flight secondary ion mass spectroscopy analysis, but not in the shoulder-affected zone or the pin-affected zone. The combined actions of both the two factors resulted in the appearance of preferential intergranular fracture in the transition zone and eventually caused the failure in the SZ. The lithium segregation at grain boundaries in the transition zone was closely associated with both the segregation in the base material and the partially dynamically recrystallized microstructure resulting from the inhomogeneous plastic deformation in the SZ.

1. Introduction

Aluminum-lithium (Al-Li) alloys has lower density, higher specific strength and specific rigidity as compared to conventional Al alloys, since each 1 wt% lithium addition reduces the density of Al alloys by 3% and increases the elastic modulus by about 6% [1]. Thus Al-Li alloys are being developed to replace conventional Al alloys, particularly for aerospace applications where weight savings are highly desirable.

Traditional technique of joining fuselage and wing structures, which are generally made of Al alloys, is riveting. The application of welding to replace riveting is an attractive option, since it allows joints with less stress concentration points and reduces the joint weight. As a innovative solid state joining technique invented by The Welding Institute of the UK, Friction stir welding (FSW) is proven to be well suited to joining Al alloys, especially high strength aerospace Al alloys that are considered non-weldable by conventional fusion welding methods [2]. Because of absence of melting and solidification processes and low heat input during FSW, gas cavities and solidification cracks are eliminated and the loss in mechanical properties as compared to the base material (BM) is much less than for fusion welding techniques [3]. Thus FSW has recently been identified as a key technology for fuselage and wing manufacturing by leading aircraft manufacturers [4] and has proved to be successful in making reliable Al-Li alloys joints [5–7].

The fracture behavior of FSW Al-Li alloy joints during tensile test has been reported in several previous studies [6,8–11]. Kroninger et al. [6] reported that for 8.1 mm thick FSW 2195-T8 Al-Li alloy joints, the tensile fracture occurred in the lowest hardness zone (LHZ), i.e., the boundary between the heat affected zone (HAZ) and the thermal mechanically affected zone (TMAZ). A similar phenomenon was found in 3.1 mm thick FSW 2198-T851 Al-Li alloy joints by Jolu et al. [9]. Recently, Mao et al. [10] indicated that the fracture locations of FSW joints of 2 mm thick 2060 Al-Li alloy plates over a wide range of

* Corresponding author.
** Corresponding author.
E-mail addresses: drni@imr.ac.cn (D.R. Ni), yszeng@hotmail.com (Y.S. Zeng).

http://dx.doi.org/10.1016/j.msea.2017.03.079
Received 1 January 2017; Received in revised form 21 March 2017; Accepted 22 March 2017
Available online 23 March 2017
0921-5093/

welding parameters were all consistent with the LHZ. However, in a study on 1 mm thick FSW 2195-T8 Al-Li alloy joints by Shukla et al. [11], failure occurred in either the stirred zone (SZ) or the LHZ, which was located in the HAZ just outside the TMAZ, during tension depending on welding parameters. Failure in the SZ was also observed in FSW joints of 12.5 mm thick 2195 Al-Li alloy plates by Hatamleh et al. [8].

For FSW joints of precipitation-hardened non-lithium containing Al alloys (2xxx, 6xxx and 7xxx), the fracture location generally corresponded to the LHZ [12–17]. However, the results in the above studies suggested that for FSW Al-Li alloy joints, both the LHZ and the SZ could be fracture location. Unfortunately, to the best of our knowledge, the exact reason for the unusual failure in the SZ instead of the LHZ for FSW Al-Li alloy joints on condition that no welding defects existed in the SZ has not been reported so far. Obviously, a systematic research aimed at elucidating the reason for the unusual failure in the SZ for FSW Al-Li alloy joints is of critical importance since it enables future weld tooling or parameter modifications to minimize the potential for failure in the SZ and may contribute to future alloy design.

In this study, 2198-T8 Al-Li alloy, which belongs to the latest generation of Al-Li alloys, was selected for FSW at 800 rpm-200 mm/min and 1600 rpm-200 mm/min. No welding defects were detected in any of the FSW joints. However, all of the joints fractured in the SZ instead of the LHZ during tensile test. Moreover, the fracture path was partially along the lazy S in the SZ, which was believed to result from oxide layer on the initial butt surface of the plates [18]. To determine whether lazy S was primarily responsible for failure in the SZ, a experimental procedure called bead-on-plate welding, i.e., a welding on a single plate without initial butt surface, was adopted since no lazy S existed in bead-on-plate welds [19]. The objective of the present work is to (a) elucidate the exact reason for the unusual failure in the SZ instead of the LHZ for FSW 2198-T8 Al-Li alloy joints and (b) analyze the influencing mechanism of the microstructure factors on fracture behavior of FSW Al-Li alloy joints.

2. Experimental procedure

3.2 mm thick 2198-T8 Al-Li alloy rolled plates with a composition of Al-0.94Li-3.37Cu-0.31Mg-0.27Ag-0.15Zr (wt%) were used in this study as the BM. Plates 75 mm in width and 300 mm in length were butt welded (hereafter referred to as butt weld) along the rolling direction (RD) using a FSW machine under welding parameters of 800 rpm-200 mm/min and 1600 rpm-200 mm/min. A tool with a concave shoulder 12 mm in diameter and a threaded cone-shaped pin 4 mm in root diameter and 3.0 mm in length was used. The plunge depth of the shoulder was controlled at ~ 0.2 mm.

For comparison, plate 150 mm in width and 300 mm in length was bead-on-plate welded (hereafter referred to as bead-on-plate weld) with the FSW running along centerline of the plate to clarify whether lazy S was primarily responsible for failure in the SZ. The welding parameters used for bead-on-plate welding process were the same as those for butt welding. It should be mentioned that both butt and bead-on-plate FSW operations were conducted under exactly the same welding conditions to ensure similar heat generation and dissipation histories.

Prior to welding, top surfaces of all the plates and butt surfaces for the butt welds were cleared by abrasive papers. The principal directions of the FSW geometry are referred to as the RD, transverse direction (TD), and normal direction (ND). All the FSW samples were naturally aged at room temperature for more than 2 months for subsequent microstructure examination, hardness and tensile tests.

Microstructure features of the welds were examined by optical microscopy (OM, Axiovert 200 MAT) and scanning electron microscopy (SEM, Quanta 600). Samples for OM and SEM were cross sectioned from the welds perpendicular to the welding direction, ground, polished and then etched using Keller's reagent (190 ml water, 2 ml hydrofluoric acid, 3 ml hydrochloric acid and 5 ml nitric acid). The precipitates and dislocation structures were characterized by transmission electron microscopy (TEM, TECNAI 20). Thin foils for TEM were prepared by jet electro-polishing using a solution of 25% nitric acid in methanol at −25 °C and 10 V.

Crystallographic texture analysis of the welds was undertaken using electron backscattered diffraction (EBSD). Sample preparation consisted of grinding and mechanically polishing, followed by electro-polishing using a solution of 30% nitric acid in methanol for 15 s at −25 °C and 12 V. Acquisition of the EBSD data was done using an FEI Sirion field-emission gun SEM equipped with a fully automatic HKL Technology EBSD attachment, operated at 20 kV. Data processing was then carried out using HKL Channel 5 software.

Time-of-flight secondary ion mass spectroscopy (TOF-SIMS) analysis was performed using an ION TOF-SIMS V in both negative and positive modes to reveal solute distribution in the SZ of the weld. TOF-SIMS samples were prepared through grinding, then mechanical polishing. Cesium ions were used for surface milling of the sample.

Vickers hardness of the welds was measured on the cross section perpendicular to the welding direction using an automatic testing machine (LECO, LM-247AT) under a load of 500 g for 10 s. First, single hardness profile from the SZ to the BM was obtained along the mid-thickness of the cross section. Then, hardness distribution map was obtained by measuring the whole cross section at an interval of 0.5 mm. Transverse tensile specimens were cut perpendicular to the welding direction using an electrical discharge machine. The configuration and size of the tensile specimen are shown in Fig. 1. The gauge part of the tensile specimen with a length of 35 mm extended from the SZ to the BM. In order to obtain the real tensile properties and fracture locations of the welds, tensile specimens were ground with SiC abrasive papers up to 800-grit to achieve a smooth surface and ensure an equal cross-sectional area at various locations of the welds. Tensile tests were carried out on a Zwick-Roell testing machine at a strain rate of 1×10^{-3} s^{-1} and three specimens were tested for each condition.

3. Results

2198-T8 Al-Li alloy plates were successfully butt welded at 800 rpm-200 mm/min and 1600 rpm-200 mm/min with defect-free welds being obtained. Lazy S was observed in the SZ for both the butt welds. Fig. 2 shows the cross-sectional macrostructure comparison between butt weld and bead-on-plate weld. It was found that lazy S was successfully eliminated in the SZ of bead-on-plate welds (Fig. 2b and d), which was consistent with the results obtained in FSW 7075Al-T651 alloy by Ren et al. [19]. In addition, the morphology and the size of the SZ were basically identical for butt welds and bead-on-plate welds (Fig. 2).

Fig. 3 shows the microhardness profile comparison between butt weld and bead-on-plate weld. It can be seen that microhardness profiles for both welds almost coincided under the investigated welding parameters. According to these results, it could be concluded that butt weld and bead-on-plate weld experienced similar deformation and thermal exposure histories since both welding procedures were conducted under exactly the same welding condition.

During tension, all of butt welds fractured in the SZ under the welding parameters investigated, with the fracture path partially along lazy S. The transverse tensile properties and fracture locations of butt

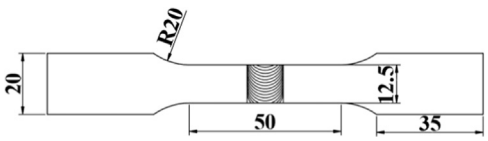

Fig. 1. Configuration and size of tensile specimen.

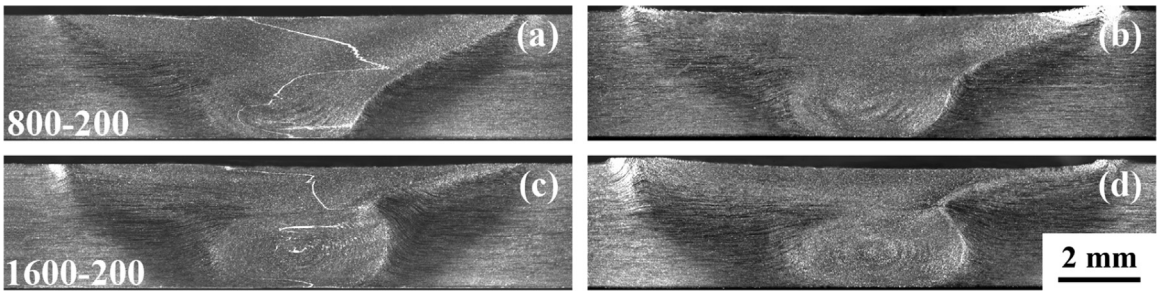

Fig. 2. Cross-sectional macrographs of FSW 2198-T8 welds (rpm-mm/min): (a) and (c) butt welds; (b) and (d) bead-on-plate welds.

welds and bead-on-plate welds are summarized in Table 1. In order to accurately locate the tensile fracture location of the welds, the cross-sections of failed specimens were etched, as shown in Fig. 4. The most striking finding was that all of bead-on-plate welds also fractured in the SZ, though lazy S did not exist in the SZ (Fig. 4b and d), indicating that lazy S was not the primary reason for failure in the SZ for FSW 2198-T8 welds.

Since both kinds of welds were subjected to similar deformation and thermal exposure condition, bead-on-plate weld specimens were used for analyzing the exact reason for failure in the SZ for FSW 2198-T8 welds so as to exclude the effect of lazy S on fracture behavior of the welds. Therefore, welds were used in the following sections to refer to bead-on-plate welds for simplification. It should be mentioned that emphasis in the current study has been placed on the unusual failure in the SZ for FSW 2198-T8 welds. Thus the variation tendency of tensile properties with welding parameter and the difference of tensile properties between butt weld and bead-on-plate weld will be discussed in detail in another article.

In order to find the essential reason for the unusual failure in the SZ, the microstructure and texture in the SZ were examined in detail. Fig. 5 shows the microstructure of the BM and SZ at 800 rpm-200 mm/min. The BM was characterized by elongated band-like grains resulting from the rolling process (Fig. 5a). It was worth noting that an inhomogeneous SZ was observed in the present FSW 2198-T8 weld (Fig. 5b-e). The longitudinal cross section (RD-ND plane) of the inhomogeneous SZ could be divided into three sub-zones (Fig. 5c), i.e. the shoulder-affected zone (zone 1), the transition zone (zone 2) and the pin-affected zone (zone 3) according to the role of the shoulder and pin in the formation of the SZ. The morphology of the transition zone was significantly different from that of the shoulder-affected zone or the pin-affected zone (Fig. 5c). The corresponding division of the transverse cross section (TD-ND plane) of the SZ is shown in Fig. 5b. Similar division of the SZ into three or two zones has been reported in several previous studies [20–22].

Closer observation revealed that both the shoulder-affected zone and the pin-affected zone consisted of fine and equiaxed fully-recrystallized grains arising from severe plastic deformation and thermal exposure during FSW (Fig. 5e) and there was no obvious difference between the two zones. However, fine recrystallized grains as well as many band-like structures (marked by arrows in Fig. 5d), which were composed of lots of coarse elongated non-recrystallized grains arranging one by one, were observed in the transition zone (Fig. 5d), indicating the occurrence of incomplete dynamic recrystallization. A similar phenomenon was also observed in the SZ at 1600 rpm-200 mm/min (not shown).

Table 1
Transverse tensile properties and fracture locations of FSW 2198-T8 welds.

Welding parameter (rpm-mm/min)	Welding procedure	UTS (MPa)	YS (MPa)	El. (%)	Fracture location
BM		488.5 ± 0.2	417.5 ± 21.9	16.9 ± 0.5	
800–200	Butt weld	397.2 ± 0.1	262.3 ± 6.5	9.1 ± 0.2	SZ
	Bead-on-plate weld	396.3 ± 3.3	274.4 ± 2.3	11.0 ± 0.4	SZ
1600–200	Butt weld	356.1 ± 4.0	262.7 ± 1.8	3.7 ± 0.0	SZ
	Bead-on-plate weld	404.9 ± 6.4	278.1 ± 5.1	10.9 ± 1.5	SZ

Fig. 6 shows the inverse pole figures from the above three zones in the SZ at 800 rpm-200 mm/min. It was found that the microtexture of the transition zone in the SZ was apparently different from that of the shoulder-affected zone or the pin-affected zone. Most of the grains in the shoulder-affected zone and the pin-affected zone exhibited orientation with their ⟨101⟩ parallel to the TD. However, orientation distribution of grains parallel to the TD was relatively diffusive in the transition zone.

Fig. 7 shows the microhardness profiles of the welds along mid-thickness of transverse cross section under different welding parameters. For the welds both at 800 rpm-200 mm/min and 1600 rpm-200 mm/min, two LHZs were clearly observed on the advancing side (AS) and the retreating side (RS) and the LHZ was located in the HAZ. In order to accurately determine the distribution of the LHZ, microhardness contour map of the weld at 800 rpm-200 mm/min is shown in Fig. 8. It was found that two LHZs did exist on both the AS and the

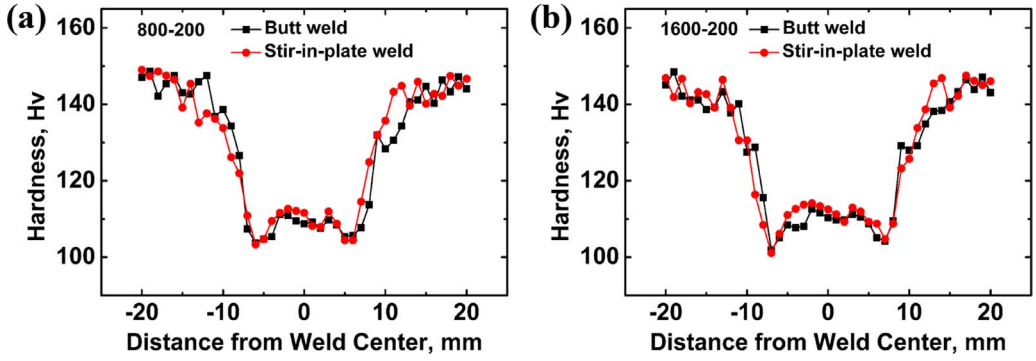

Fig. 3. Comparison of microhardness profiles between butt weld and bead-on-plate weld at (a) 800 rpm-200 mm/min and (b) 1600 rpm-200 mm/min.

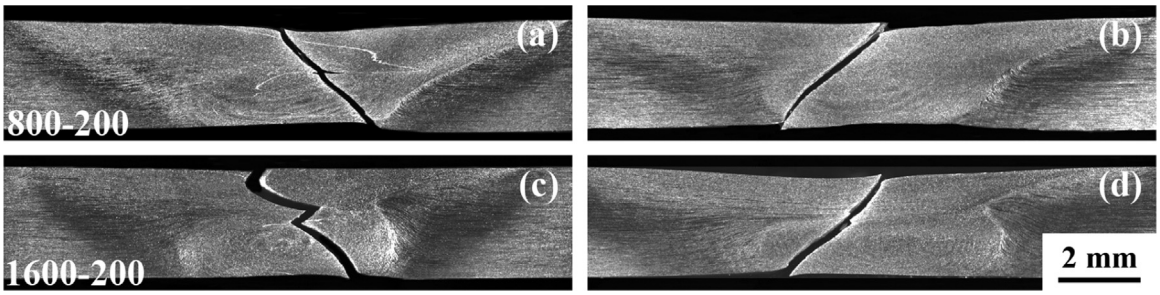

Fig. 4. Fracture locations of FSW 2198-T8 welds (rpm-mm/min): (a) and (c) butt welds; (b) and (d) bead-on-plate welds.

RS. It can be determined that the LHZ was indeed located in the HAZ instead of the SZ and was about a 45° angle to the tensile axis. Since all of the FSW 2198-T8 welds failed in the SZ (Fig. 4), the fracture location did not correspond to the LHZ, which was different from fracture behavior of FSW joints of conventional precipitation-hardened Al alloys [12–17]. For the weld at 1600 rpm-200 mm/min, its micro-

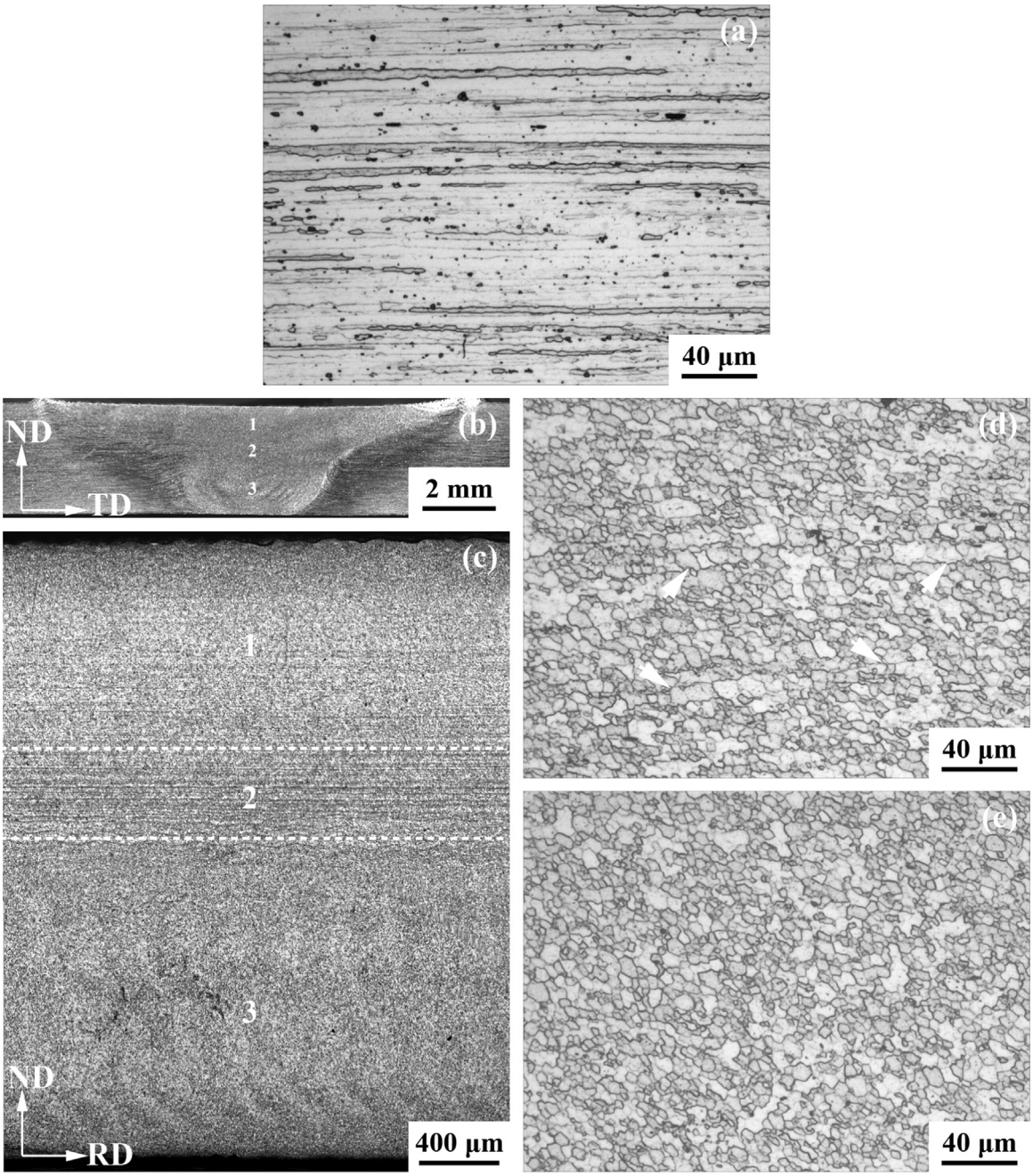

Fig. 5. Optical micrographs of weld (800 rpm-200 mm/min): (a) BM; (b) transverse cross section and (c) magnified longitudinal cross section of SZ, (d) and (e) magnified images of positions 2 and 3 in Fig. 5b.

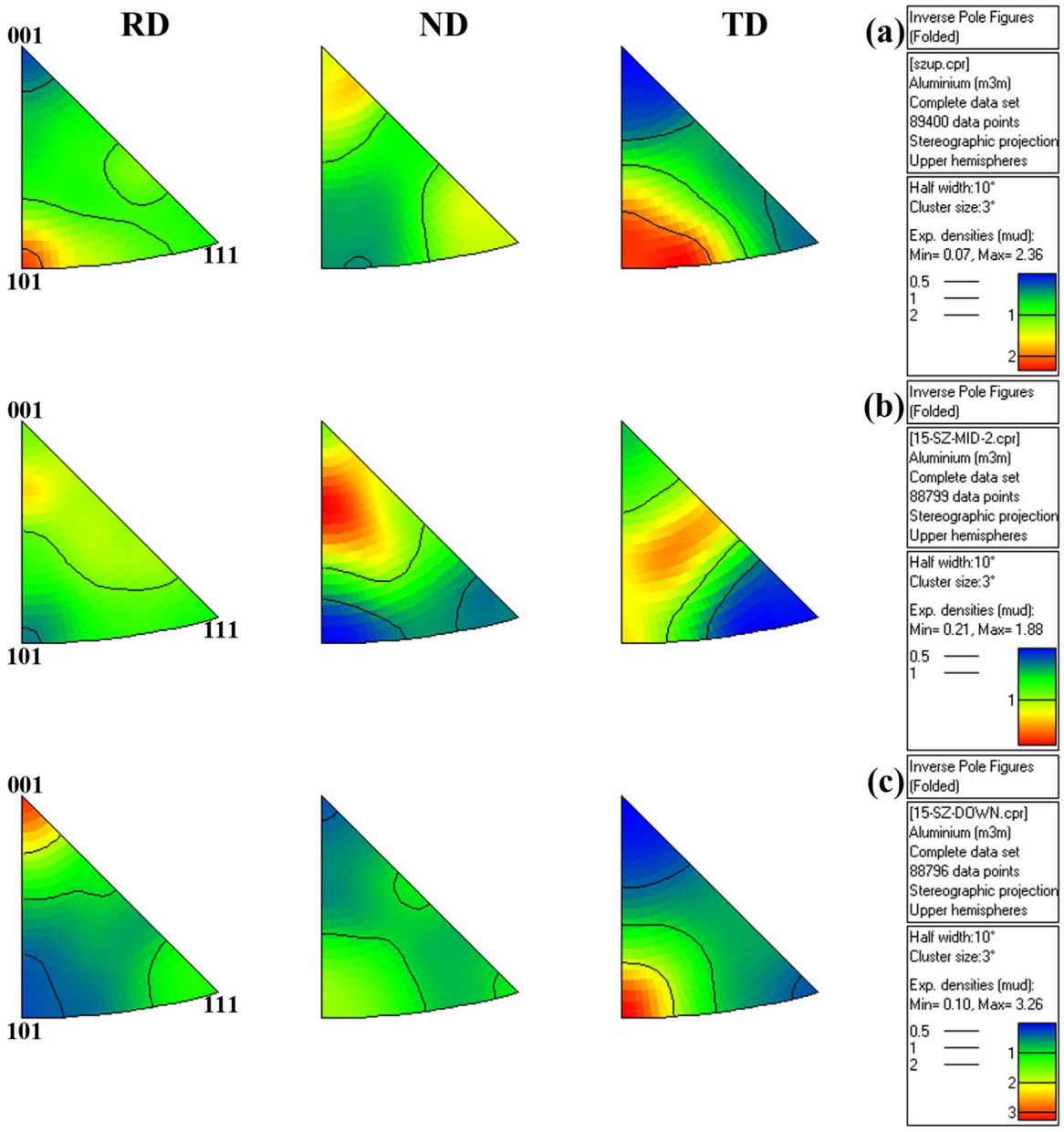

Fig. 6. Inverse pole figures from SZ (800 rpm-200 mm/min): (a) shoulder-affected zone, (b) transition zone and (c) pin-affected zone.

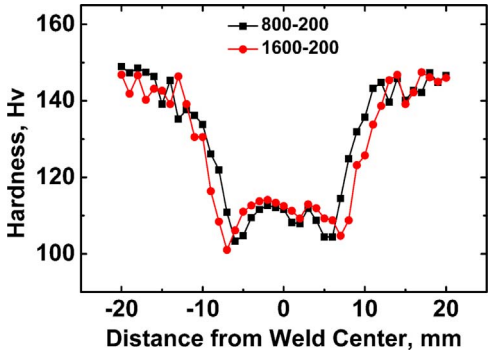

Fig. 7. Microhardness profiles of welds under different welding parameters (rpm-mm/min).

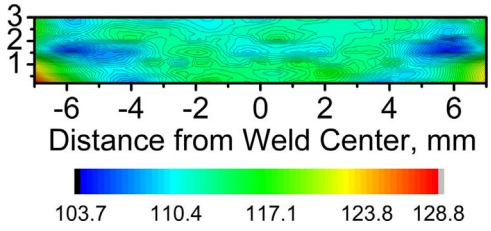

Fig. 8. Microhardness contour map of weld (800 rpm-200 mm/min).

hardness contour map was similar to that of the weld at 800 rpm-200 mm/min and is therefore not shown.

In order to find out the crack initiation site of the weld during tension, the weld was tensile deformed until the stress dropped down after having reached the ultimate tensile strength (UTS), followed by unloading before failure. The SEM microstructures of the SZ of tensile deformed weld at 800 rpm-200 mm/min are shown in Fig. 9. It was noted that crack initiated preferentially in the transition zone in SZ during tension (marked by rectangle in Fig. 9a, magnified image shown in Fig. 9b). Furthermore, closer observation of the crack initiation site revealed that crack initiated in an intergranular manner (marked by arrows in Fig. 9c).

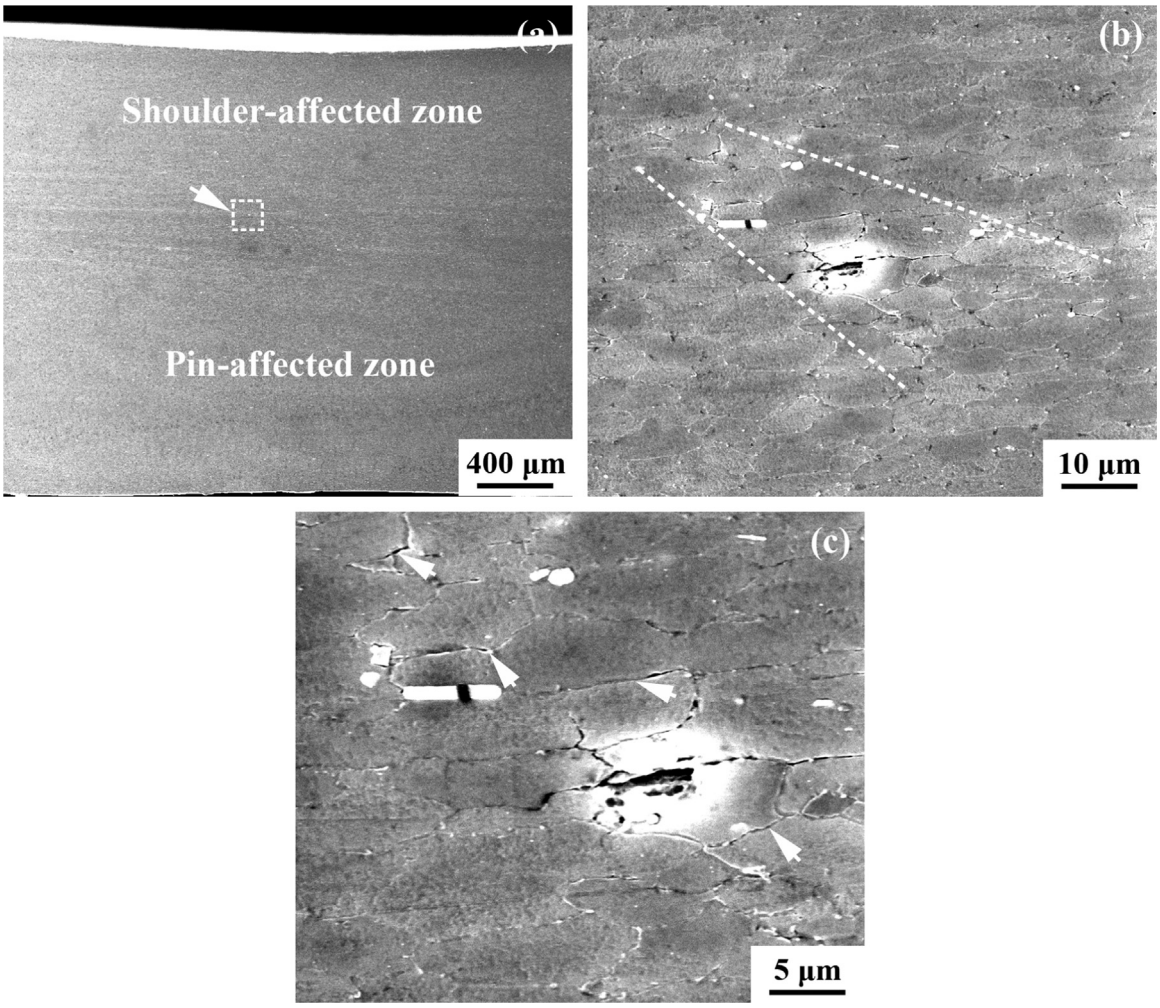

Fig. 9. (a) SEM micrograph of SZ of tensile deformed weld showing crack initiation site (800 rpm-200 mm/min), (b) magnified image of rectangle area in Fig. 9a and (c) further magnified image of area between dotted lines in Fig. 9b.

Fig. 10 shows the optical micrographs of the transition zone in SZ for failed weld at 800 rpm-200 mm/min. Intergranular fracture grains (marked by arrows in Fig. 10b) were distinctly visible in some regions in the transition zone (position B in Fig. 10a), which was consistent with the results shown in Fig. 9c. Besides, transgranular fracture grains (marked by arrows in Fig. 10c) were also observed in other regions in the transition zone (position C in Fig. 10a), indicating mixed fracture of both transgranular and intergranular rupture.

Fig. 11 shows the optical micrographs of the pin-affected zone in the SZ for failed weld at 800 rpm-200 mm/min. It was noted that merely transgranular fracture grains were detected in the pin-affected zone (marked by arrows in Fig. 11b), suggesting simple transgranular fracture for this zone. The fracture feature of the shoulder-affected zone was similar to that of the pin-affected zone (not shown). Thus the fracture behavior of the transition zone in the SZ was clearly different from that of the shoulder-affected zone or the pin-affected zone.

4. Discussion

4.1. Origin of preferential crack initiation in transition zone

As shown in Fig. 6, the transition zone in the SZ exhibited different microtexture as compared to the shoulder-affected zone or the pin-affected zone. It is well known that the crystallographic orientation distributions influence the plastic deformation abilities of materials because plastic deformation arises from the slip on the closest-packing plane with the maximum critical resolved shear stresses in Al alloys. Thus the local microtexture distribution in the SZ suggests that it has a local distribution of plastic deformation ability.

In order to assess the deformation ability of the above three zones in the SZ, grain-specific Taylor factors (M) for these zones were computed according to the EBSD results. M for uniaxial deformation could be expressed as follows: $M = \sigma/\tau_c$ [23]. The σ is the flow stress under uniaxial loading and the τ_c is the resolved shear stress working on the active slip system. Thus M is a function of the grain crystallographic orientation as well as the imposed stress. A smaller M indicates that a larger τ_c works on the activated slip system, i.e., grains with smaller M are deformed more easily.

Fig. 12 shows the M distribution maps in the above three zones in the SZ at 800 rpm-200 mm/min for uniaxial tension in the TD. In the M maps, grains with smaller M were shaded with a heavier shade of gray. Obviously, the transition zone in the SZ had a larger area fraction of grains with small M values than the shoulder-affected zone and the pin-affected zone (Fig. 12a-c). For comparison, M for the LHZ were also computed (Fig. 12d). Average M values in the shoulder-affected zone, the transition zone, the pin-affected zone and LHZ were 3.27, 3.03, 3.27 and 3.43, respectively. This result indicated that under the same uniaxial tensile stress in the TD, all of the three zones in the SZ had a larger τ_c working on the slip system than the LHZ. Meanwhile, among the three zones in the SZ, the transition zone had a largest τ_c working on the slip system. This suggested that plastic deformation should take place in the transition zone more easily than in other zones

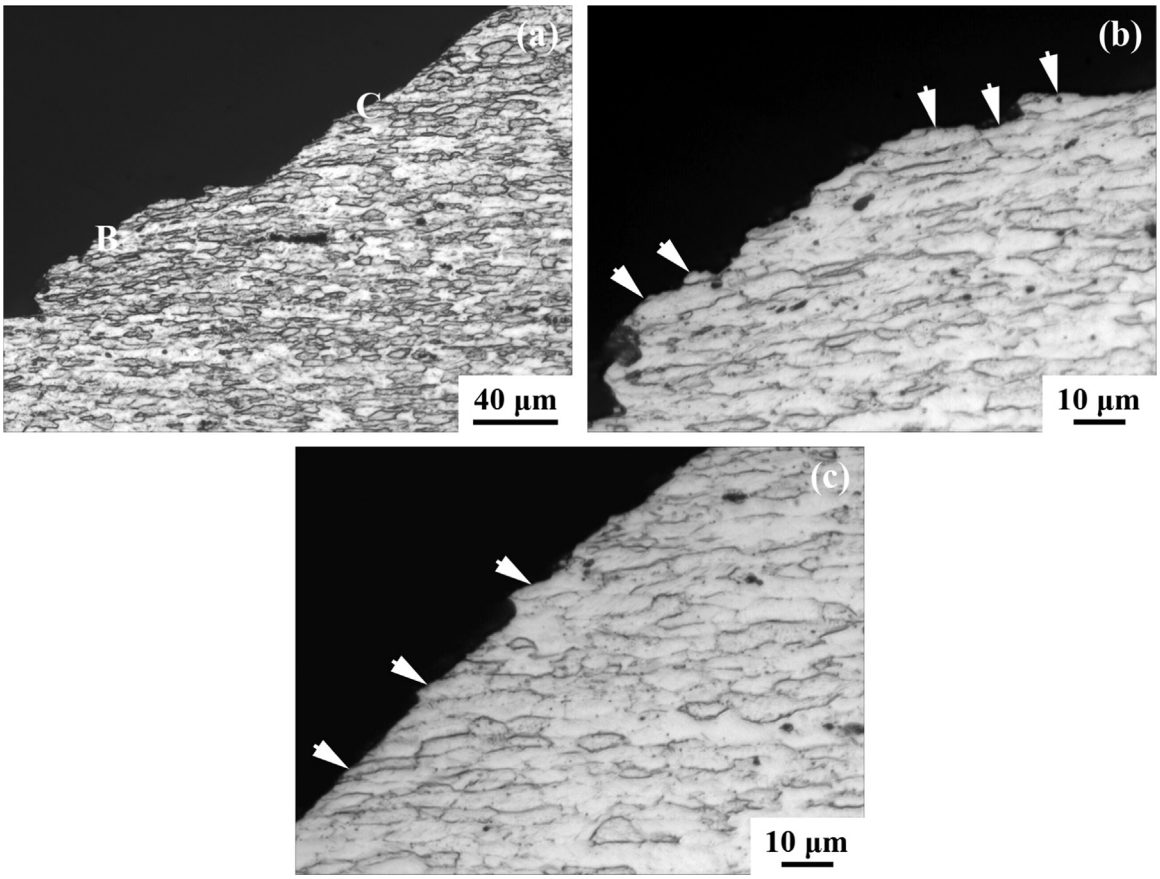

Fig. 10. Optical micrographs of failed weld (800 rpm-200 mm/min): (a) the transition zone in SZ, (b) and (c) magnified images of positions B and C in Fig. 10a.

in the SZ or in the LHZ, which led to preferential crack initiation in the transition zone during tension of the weld.

The correlation between M distribution and tensile fracture location of FSW joints has been reported previously by Sato et al. [24] and Tayon et al. [25]. Sato et al. [24] found that for FSW 6063Al-T5 joint, two kinds of fracture locations were observed depending on the hardness distribution across the weld. In a joint having heterogeneous hardness profile, such as an as-welded weld, fracture occurred in the LHZ. When a joint had homogeneous hardness profile, such as a postweld solution heat-treated and aged weld, it fractured in the region with a minimum average M value. Tayon et al. [25] showed that for FSW 2195-O Al-Li alloy joint followed by postweld T8 heat-treatment, failure was located in a visible band of low M grains in the TMAZ on the assumption that precipitate distribution was uniform across the weld.

4.2. Origin of intergranular fracture in transition zone

The use of Al-Li alloys in aerospace industries has not been so wide as was anticipated during the alloy-development programs in the 1980s [26]. Several factors hindered the application of AI-Li alloys and one of them was their poor short-transverse fracture toughness and ductility, which was due to their greater tendency for intergranular fracture as compared with conventional Al alloys [26]. Reasons for intergranular fracture in Al-Li alloys have been reported previously by many investigators and different explanations were put forward in these studies [26–34]. In general, the proposed explanations for intergranular fracture in Al-Li alloys could be classified into the following five viewpoints.

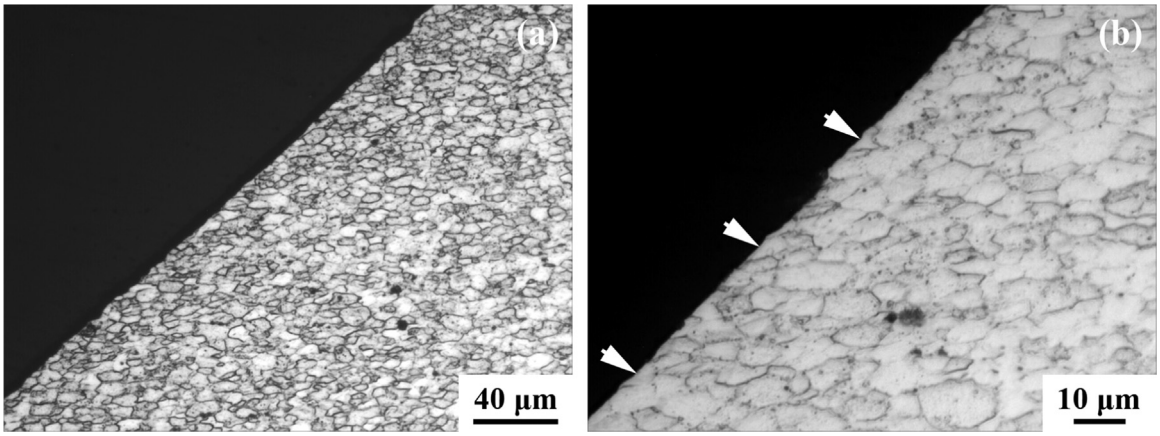

Fig. 11. Optical micrographs of failed weld (800 rpm-200 mm/min): (a) pin-affected zone in SZ and (b) magnified image of Fig. 11a.

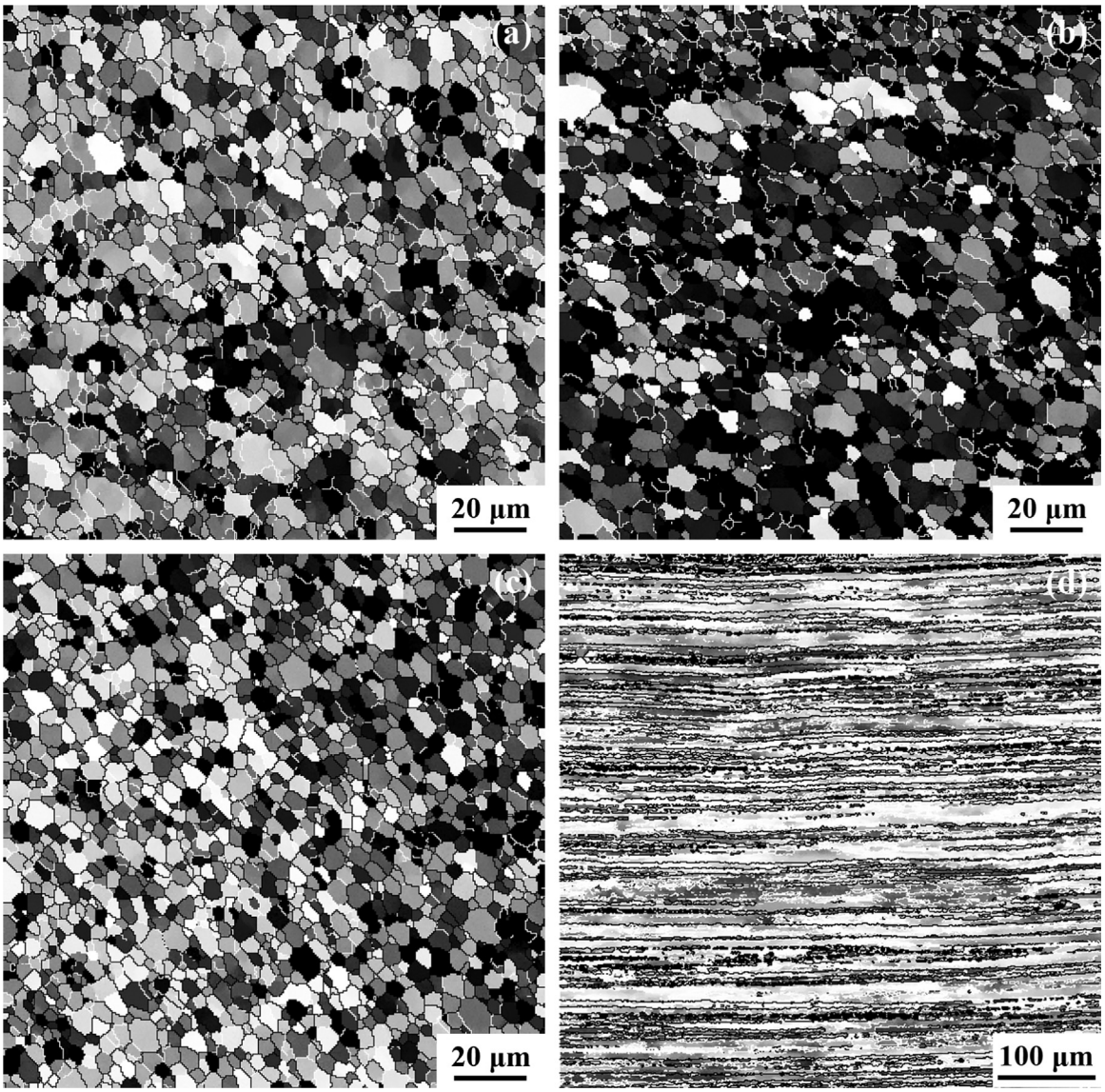

Fig. 12. Taylor factor M distributions for uniaxial tension in TD (800 rpm-200 mm/min): (a) shoulder-affected zone, (b) transition zone and (c) pin-affected zone in SZ; (d) LHZ.

4.2.1. Presence of grain boundary precipitates and precipitate free zones (PFZs)

The presence of grain boundary precipitates and PFZs adjacent to grain boundaries undoubtedly facilitated intergranular fracture in AI-Li alloys, due to strain localization in soft PFZs and nucleation of voids at grain boundary precipitates [34]. Dimpled intergranular fracture occurred as a consequence of growth and coalescence of these voids [34].

4.2.2. Hydrogen segregation at grain boundaries

Hydrogen segregation at grain boundaries was also a well-known cause of intergranular fracture in most alloys including Al alloys. Absorption of hydrogen in Al alloys occurred as a result of reaction of the melt with moisture in the atmosphere during melting. Al-Li alloys normally contained higher levels of hydrogen than conventional Al alloys owing to the strong affinity between hydrogen and lithium [27]. However, a recent detailed investigation by Bennett et al. [27] indicated that hydrogen did not exert a substantial effect on short-transverse fracture toughness and intergranular fracture resistance of a 2090 Al-Li alloy extrusion, since hydrogen was presented as discrete lithium hydride particles at grain boundaries, along with numerous other grain boundary precipitates, rather than segregated as solute along grain boundaries.

4.2.3. Alkali-metal-impurity (AMI) phases segregation at grain boundaries

The effect of AMI phases on fracture toughness of 2090 Al-Li alloy extrusions has been systematically investigated by Sweet et al. [33]. It was reported that liquid Na-K-rich phases were detected at grain boundaries using TEM in 2090 Al-Li alloy with very high AMI contents. Fractographic observations revealed that the presence of grain boundary AMI phases (≥5–10 ppm) could result in intergranular fracture due to liquid-metal embrittlement. However, there was no evidence of significant embrittlement in commercial Al-Li alloys where AMI levels were generally ≤5 ppm [33].

4.2.4. Planar slip

Al-Li alloys were apt to planar slip when coherent δ′ (Al_3Li) precipitates were present as main strengthening precipitates because coherent δ′ precipitates were easily sheared by dislocations, thereby facilitating subsequent slip on the same slip plane. Planar slip was the most often cited opinion for intergranular fracture in Al-Li alloys and it was suggested that planar slip bands impinging upon grain boundaries could produce locally great stress concentrations and thus promoted intergranular fracture [28,32]. However, it should be mentioned that stresses due to planar slip bands impinging upon grain boundaries

could probably be relieved by slip in the soft PFZs or adjacent grains and thus planar slip bands did not necessarily lead to high stress concentrations at grain boundaries. In a study on 8090 Al-Li alloy, Lynch et al. [31] found that re-ageing 8090-T8771 plate (aged 32 h at 170 °C) for 5 min at 200 °C doubled the short-transverse fracture toughness and eliminated intergranular fracture. Nevertheless, this re-aging treatment produced no marked change in microstructural features with only reversion of some of the finest δ′ precipitates. Furthermore, no significant differences in the degree of planar slip were observed between single-aged material and double-aged material. Thus there was no evidence from their study that planar slip facilitated intergranular fracture [31]. Therefore, it was debatable whether planar slip contributed significantly to intergranular fracture in Al-Li alloys.

4.2.5. Lithium segregation at grain boundaries

Lithium segregation at grain boundaries as a prime cause of intergranular fracture in Al-Li alloys gradually drew more and more attention of investigators [29–31]. Lynch et al. [29,31] pointed out that lithium segregation at grain boundaries was mainly responsible for intergranular fracture and low toughness in a single-aged (T8771) commercial 8090 Al-Li alloy plate and that re-aging for short times at higher temperatures than the first ageing treatment substantially increased toughness and eliminated intergranular fracture by decreasing the extent of lithium segregation. In another study, Lynch et al. [30] found that for a naturally aged 8090 Al-Li alloy plate, the extent of intergranular fracture was greater and toughness was lower for near surface position compared with mid-thickness position. They suggested that such phenomenon was attributed to more lithium segregation at grain boundaries closer to the surface of plate due to greater portion of high-angle grain boundaries since lithium segregation was more stable at grain boundaries with higher misorientations.

Recently, the relative importance of the five reasons for intergranular fracture in Al-Li alloys as mentioned above has been discussed in detail by Pasang et al. [26]. It was concluded that lithium segregation at grain boundaries rather than planar slip was primarily responsible for intergranular fracture in Al-Li alloys, contrary to wide-spread viewpoint. However, the low atomic number of lithium as well as presence of lithium-rich grain boundary precipitates made the observation of lithium segregation at grain boundaries very difficult [26]. To the best of our knowledge, the only direct evidence for lithium segregation at grain boundaries was obtained by Lynch et al. [31]. In their study, analytical TEM (using plasmon-peak energies obtained from parallel electron energy loss spectra to measure lithium concentrations) revealed that lithium segregation developed at grain boundaries in 8090 Al-Li alloy. However, plasmon peak energy shifts across grain boundaries were converted to lithium concentrations on the assumption that other elements did not contribute to the shifts [31].

In the following section, the five possible reasons as aforementioned were discussed one by one to seek out the exact reason for intergranular fracture in the transition zone in the SZ of FSW 2198-T8 welds. Microstructure of the shoulder-affected zone, transition zone and pin-affected zone in the SZ were carefully examined by TEM. No grain boundary precipitates or PFZs were detected in any of the three zones and typical TEM microstructure is shown in Fig. 13a. This observation indicated that presence of grain boundary precipitates and PFZs could be ruled out as a cause of intergranular fracture in this study.

Fig. 13b shows the bright field TEM image of the SZ depicting precipitate distribution in the interior of grains. Lots of fine δ′ precipitates with coherent strain contrast (marked by arrows in Fig. 13b) were observed in the SZ. The coherence of δ′ precipitates was further confirmed by the superlattice reflections in the selected area electron diffraction pattern taken in a ⟨001⟩Al zone axis (insert in Fig. 13b). To determine whether planar slip occurred in the SZ during tension, the above three zones in the SZ from a tensile deformed weld, which was loaded to the same extent as that for the observation of crack initiation (Fig. 9), were subjected to TEM observation. It was surprising that no planar slip bands or traces of planar slip were found in the SZ. Instead, a high density of dislocations was fairly homogeneously distributed in most areas of the SZ and typical TEM microstructure is shown in Fig. 13c. Thus the role of planar slip in producing intergranular fracture could be excluded.

It was interesting that planar slip did not occur in the SZ during tension when coherent δ′ precipitates presented as main strengthening precipitates (Fig. 13b and c). In a study on Al-Li-Cu-X alloys, Csontos et al. [28] reported that the larger slip length, i.e. larger grain size, greatly increased the intensity of planar slip. In other words, microstructure with smaller grain size in the SZ in this study was not beneficial to planar slip. This was because grain refinement decreased the slip length, leading to reduced dislocation pile-up stresses at grain boundaries, and thus encouraged multiple slip and promoted homogeneous deformation [34].

To verify the hypotheses for intergranular fracture based on hydrogen or AMI phases or lithium segregation at grain boundaries, SIMS was employed to investigate the distribution of solutes in the shoulder-affected zone, the transition zone and the pin-affected zone in the SZ and SIMS mapping results are shown in Fig. 14. It can be seen that obvious lithium segregation at grain boundaries occurred in the transition zone in the SZ (marked by arrows in Fig. 14b). However, lithium was homogeneously distributed in both the shoulder-affected zone and the pin-affected zone (Fig. 14a and c). Besides, no evidence of hydrogen or AMI element (not shown here) enrichment at grain boundaries was detected throughout the microstructure of the above three zones in the SZ (Fig. 14a-c), indicating that the hypotheses for intergranular fracture based on hydrogen or AMI phase effects could be eliminated.

Therefore, it can be concluded on the basis of the above observations that lithium segregation at grain boundaries was responsible for intergranular fracture in the transition zone in the SZ for FSW 2198-T8 welds. It should be mentioned that this is the first time that lithium segregation at grain boundaries in Al-Li alloys was directly observed by SIMS, as far as the authors are aware.

Attempts to obtain direct evidence of lithium segregation at grain boundaries by SIMS have been made previously by several investigators [29,35]. SIMS technique was employed to investigate the distribution of solutes within a electrospark deposited material of 2199 Al-Li alloy by Heard et al. [35] and the results revealed a homogeneous distribution of lithium as well as other elements throughout the microstructure. It was noted that the outline of grains was clearly distinguished in the SIMS mapping of the present work (Fig. 14) since the secondary-ion signal for an element depends on the crystallographic orientation of the surface, while it could not be observed in the SIMS mapping of their study [35]. The precise reasons for this difference were not known, but one possible explanation was the adoption of different ions which were used for surface milling of SIMS sample. In the study on 8090 Al-Li alloy plate by Lynch et al. [29], SIMS observations on freshly produced intergranular fracture surface of single-aged (T8771) material failed to reveal any evidence of lithium enrichment at grain boundaries, though other indirect observations suggested that lithium segregation at grain boundaries was mainly responsible for intergranular fracture in single-aged material. Since surface lithium atoms could diffuse or be oxidized after fracture, evidence of lithium segregation on fracture surface might be very difficult to detect [31].

According to the discussions mentioned above, the average M value and solute distribution in the transition zone in the SZ were quite different from those in the shoulder-affected zone and the pin-affected zone (Figs. 12 and 14). The transition zone had the smallest M value (Fig. 12) which resulted in an area that was crystallographically weak, i.e. plastic deformation should take place more easily in this zone. Meanwhile, the transition zone exhibited distinct lithium segregation at grain boundaries (Fig. 14b) which should weaken interatomic bonds

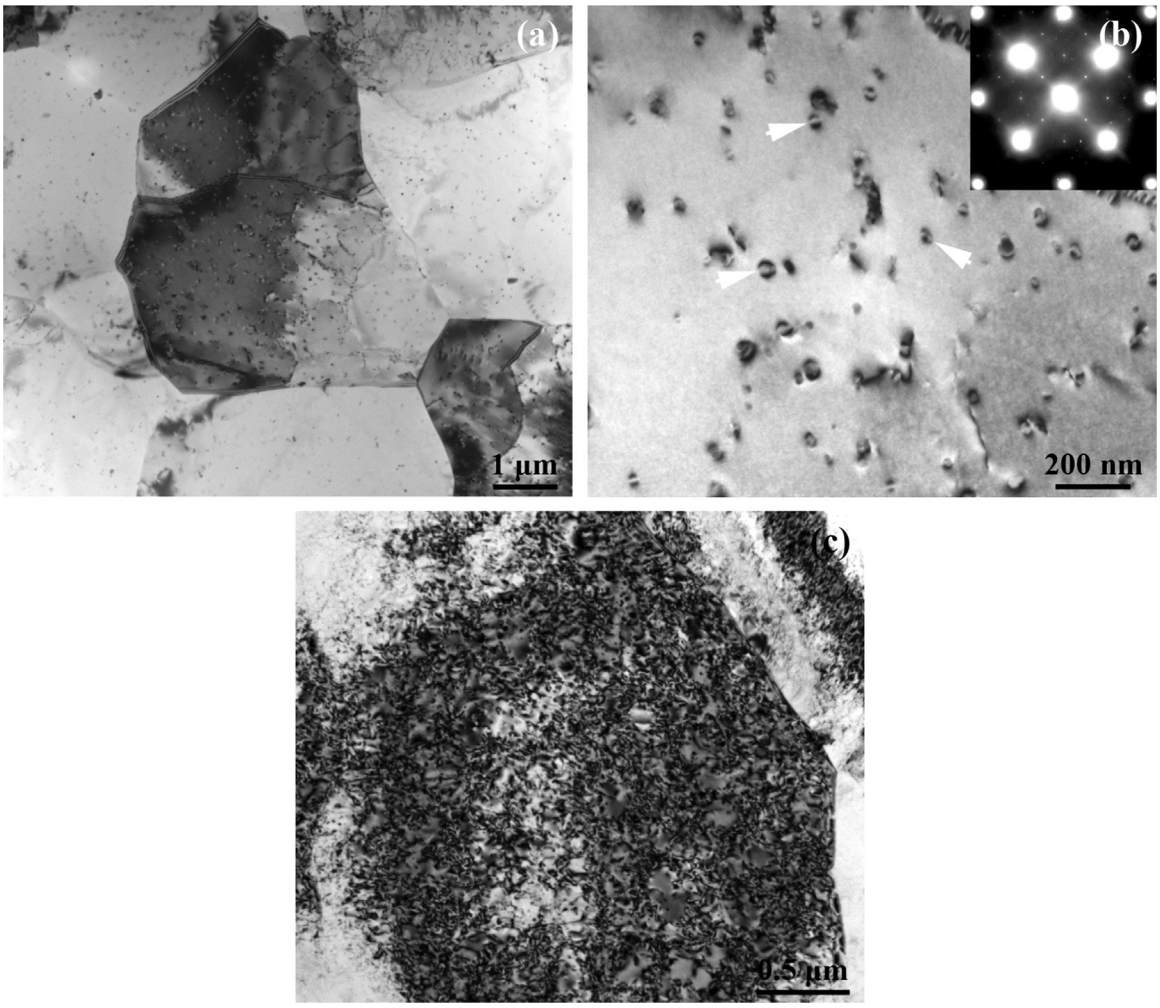

Fig. 13. Bright field TEM micrographs of SZ (800 rpm-200 mm/min): (a) and (b) images from weld before tension showing grain structure and precipitates, respectively; (c) image from tensile deformed weld showing dislocation structure.

[36]. The combined actions of both the two factors would facilitate intergranular fracture in the transition zone in the SZ during tension (Fig. 10b) and eventually causing failure in the SZ (Fig. 4).

4.3. Reason for formation of inhomogeneous SZ

4.3.1. Reason for partially dynamically recrystallized microstructure in transition zone

During FSW process, the material underwent intense plastic deformation at elevated temperature, resulting in generation of microstructure that was characterized by fine and equiaxed recrystallized grains in the SZ, as observed in the shoulder-affected zone and the pin-affected zone (Fig. 5e). However, it was surprising that incompletely dynamically recrystallized microstructure consisting of both fine recrystallized grains and coarse elongated non-recrystallized grains was observed in the transition zone (Fig. 5d) for the alloy and welding conditions in the present study. Since the dynamic recrystallization process was strongly affected by the extent of deformation, the occurrence of partially recrystallized zone suggested that plastic deformation might not be homogeneously distributed during FSW.

In a study on FSW 6061Al-T6 joints, Xu et al. [21] reported the equivalent plastic strain contours of the joint based on the results of finite-element simulations of the FSW process. By correlating the distribution of equivalent plastic strain with the texture pattern on transverse cross section of the SZ, one could find that the smallest equivalent plastic strain occurred in a region between the shoulder-affected zone near the top surface of the SZ and the pin-affected zone where a banded texture pattern existed, i.e., the transition zone as called in the present study. Colligan et al. [37] investigated the material flow behavior during FSW of 6061Al-T6 and 7075Al-T6 plates via steel shot tracer technique. Line of small steel balls were embedded along the welding direction at different positions within the joints. They found that not all the material in the tool path was actually stirred. Instead, quite a large amount of the material was simply extruded around the retreating side of the rotating tool pin and deposited behind.

The results in the above studies [21,37] indicated that an inhomogeneous distribution of plastic deformation did occur within the SZ during the FSW process. The elongated band-like grains in the BM (Fig. 5a) were involved in the SZ under the stirring action of the rotating tool. Due to the relatively lower extent of plastic deformation in the transition zone in the SZ during FSW [21], dynamic recrystallization did not occur completely in this zone and thus part of the microstructure features of the BM were retained, leading to the formation of band-like structure containing lots of coarse elongated non-recrystallized grains (marked by arrows in Fig. 5d) in this zone. The inhomogeneous microstructure of the SZ has also been observed in FSW 2195 Al-Li alloy joint by Fonda et al. [38]. They reported that some substructure in the form of nearly parallel bands of finer grains was evident at the center of the SZ, but the origin of this banding was not provided in their study.

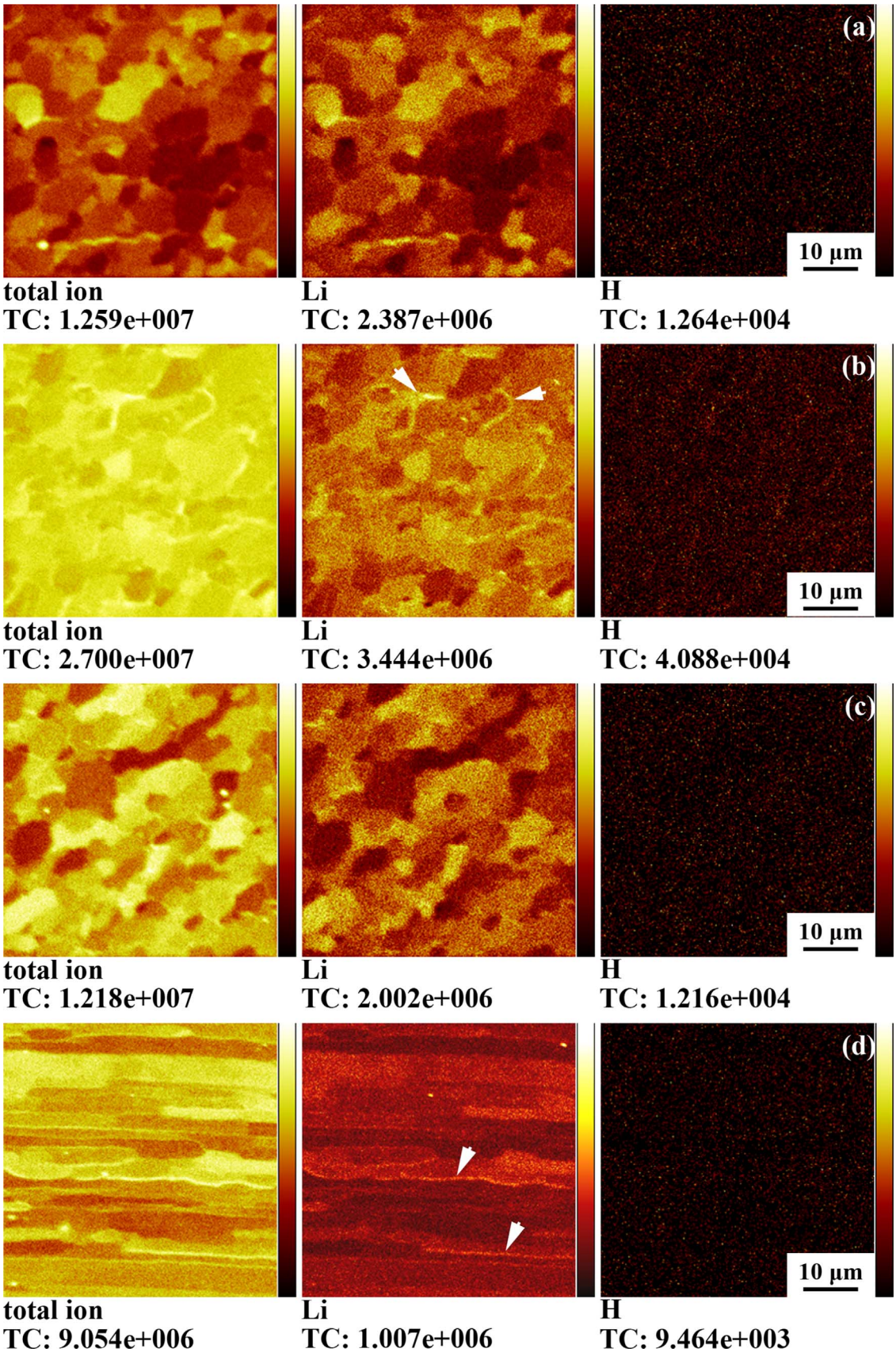

Fig. 14. TOF-SIMS mapping of solute distribution (800 rpm-200 mm/min): (a) shoulder-affected zone, (b) transition zone and (c) pin-affected zone in SZ; (d) BM.

4.3.2. Reason for lithium segregation at grain boundaries in transition zone

Lithium segregation occurred mainly during the primary ageing treatment [26]. Lynch et al. [29,31] reported that re-ageing 8090-T8771 Al-Li alloy plate for short times at temperatures above the first aging temperature decreased the extent of lithium segregation at grain boundaries by producing rapid grain boundary diffusion of the segregated lithium to grain boundary precipitates and thus resulted in a dramatic increase of the short-transverse fracture toughness. SIMS mapping results depicting solute distribution in the BM are shown in Fig. 14d. It was noted that distinct lithium segregation at grain boundaries existed in the BM (marked by arrows in Fig. 14d), which possibly originated from the primary ageing treatment (T8) during the manufacturing process [26].

Under the stirring action of the rotating tool, the material within the SZ experienced severe plastic deformation and significant high-temperature exposure. A temperature rise of about 400–550 °C has been recorded within the weld during FSW Al alloys [39,40] due to the enhanced friction between tool and workpiece and plastic deformation of workpiece. Such intense plastic deformation and temperature rise within the SZ would result in breakup, dispersion and subsequently dissolution of the segregated lithium at grain boundaries of the BM. The released lithium were redistributed throughout the entire SZ in the form of either solute lithium in supersaturated solid solution in the Al matrix or δ′ precipitates in the recrystallized grain interiors which re-precipitated during natural aging.

However, the relatively lower extent of plastic deformation in the transition zone in the SZ [21] resulted in occurrence of incomplete dynamic recrystallization as mentioned above (Fig. 5d) and thus led to inheritance of part of the microstructure feature of the BM, i.e. part of the lithium segregation at grain boundaries of the BM were retained in the transition zone. In the meantime, although the SZ experienced significant high-temperature exposure [39,40], the thermal cycle was very short [41,42] as a result of the relatively rapid heating and cooling process during FSW due to fast traveling of the rotating tool. It was speculated that such a short thermal cycle during FSW might not allow sufficient reversion of lithium segregation at grain boundaries in the transition zone by diffusion of grain boundary lithium atoms. Thus obvious lithium segregation at grain boundaries occurred in the transition zone (marked by arrows in Fig. 14b), whereas no evidence of lithium enrichment at grain boundaries was detected in both the shoulder-affected zone and the pin-affected zone (Fig. 14a and c).

The results of the current study indicate that the fracture behavior of FSW Al-Li alloy joints are sensitive to several microstructural features, such as crystallographic orientation of grains, solute distribution, grain size, precipitate distribution, etc. Both the grains with low M values and lithium segregation at grain boundaries weakened the mechanical properties of the transition zone in the SZ, eventually causing failure in the SZ for FSW 2198-T8 welds. Therefore the SZ may be the weakest zone. Thus, both the LHZ and SZ should be taken into consideration in determining fracture location of FSW 2198-T8 welds. Since the presence of the local soft zone (the transition zone) in the SZ results in unusual failure of the welds during tension, a complete understanding of material flow throughout the SZ, particularly in the transition zone, during FSW deserves further investigation.

5. Conclusions

(1) 3.2 mm thick rolled 2198-T8 Al-Li plates were successfully friction stir welded at 800 rpm-200 mm/min and 1600 rpm-200 mm/min, obtaining defect-free joints. However, all of the joints fracture in the SZ rather than the LHZ, which was different from the typical fracture behavior of FSW joints of conventional precipitation-hardened Al alloys.

(2) A experimental procedure called bead-on-plate welding was adopted to exclude the effect of lazy S on fracture behavior of the welds. Comparison of fracture locations between butt welds and bead-on-plate welds indicated that lazy S was not primarily responsible for the unusual fracture in the SZ.

(3) An inhomogeneous SZ was observed in FSW 2198-T8 welds, which could be divided into three subzones, i.e., the shoulder-affected zone, the pin-affected zone and the transition zone between the above two zones. Both the shoulder-affected zone and the pin-affected zone were composed of fine and equiaxed recrystallized grains. However, fine grains as well as coarse elongated non-recrystallized grains were detected in the transition zone, indicating the occurrence of incomplete dynamic recrystallization.

(4) The smallest Taylor factor was obtained in the transition zone as compared with other two zones in the SZ, indicating that plastic deformation should take place more easily in this zone during tension. In addition, the transition zone exhibited distinct lithium segregation at grain boundaries, whereas no evidence of lithium enrichment was detected in the shoulder-affected zone or the pin-affected zone. Both the above two factors contributed to preferential intergranular fracture in the transition zone and subsequently resulted in fracture in the SZ.

(5) The BM exhibited lithium segregation at grain boundaries and during FSW process, part of the segregated lithium were retained in the partially dynamically recrystallized microstructure in the transition zone. Meanwhile, the thermal cycle of FSW was too short to enable sufficient diffusion of segregated lithium at grain boundaries, and thus obvious lithium segregation occurred in the transition zone.

Acknowledgements

This work was supported by the National Natural Science Foundation of China under grant Nos. 51331008.

References

[1] K.K. Sankaran, N.J. Grant, Mater. Sci. Eng. 44 (1980) 213–227.
[2] R.S. Mishra, Z.Y. Ma, Mater. Sci. Eng. R 50 (2005) 1–78.
[3] P.L. Threadgill, A.J. Leonard, H.R. Shercliff, P.J. Withers, Int. Mater. Rev. 54 (2009) 49–93.
[4] T. Dursun, C. Soutis, Mater. Des. 56 (2014) 862–871.
[5] J. Altenkirch, A. Steuwer, P.J. Withers, Sci. Technol. Weld. Join. 15 (2010) 522–527.
[6] H.R. Kroninger, A.P. Reynolds, Fatigue Fract. Eng. Mater. 25 (2002) 283–290.
[7] S.M.O. Tavares, J.F. dos Santos, P. de Castro, Theor. Appl. Fract. Mec. 65 (2013) 8–13.
[8] O. Hatamleh, Int. J. Fatigue 31 (2009) 974–988.
[9] T. Le Jolu, T.F. Morgeneyer, A.F. Gourgues-Lorenzon, Sci. Technol. Weld. Join. 15 (2010) 694–698.
[10] Y.Q. Mao, L.M. Ke, F.C. Liu, C.P. Huang, Y.H. Chen, Q. Liu, Int. J. Adv. Manuf. Technol. 81 (2015) 1419–1431.
[11] A.K. Shukla, W.A. Baeslack, Sci. Technol. Weld. Join. 14 (2009) 376–387.
[12] R.W. Fonda, J.F. Bingert, Metall. Mater. Trans. A 35A (2004) 1487–1499.
[13] B. Heinz, B. Skrotzki, Metall. Mater. Trans. B 33B (2002) 489–498.
[14] K.V. Jata, K.K. Sankaran, J.J. Ruschau, Metall. Mater. Trans. A 31A (2000) 2181–2192.
[15] P. Moreira, T. Santos, S.M.O. Tavares, V. Richter-Trummer, P. Vilaca, P. de Castro, Mater. Des. 30 (2009) 180–187.
[16] W.F. Xu, J.H. Liu, G.H. Luan, C.L. Dong, Mater. Des. 30 (2009) 3460–3467.
[17] A.A. Zadpoor, J. Sinke, R. Benedictus, R. Pieters, Mater. Sci. Eng. A 494 (2008) 281–290.
[18] Y.S. Sato, F. Yamashita, Y. Sugiura, S.H.C. Park, H. Kokawa, Scr. Mater. 50 (2004) 365–369.
[19] S.R. Ren, Z.Y. Ma, L.Q. Chen, Mater. Sci. Eng. A 479 (2008) 293–299.
[20] M.M.Z. Ahmed, B.P. Wynne, W.M. Rainforth, P.L. Threadgill, Mater. Charact. 64 (2012) 107–117.
[21] S.M. Xu, X.M. Deng, Acta Mater. 56 (2008) 1326–1341.
[22] Z. Zhang, B.L. Xiao, Z.Y. Ma, Mater. Sci. Eng. A 614 (2014) 6–15.
[23] C.J. Dawes, W.M. Thomas, Weld. J. 75 (1996) 41–45.
[24] Y.S. Sato, H. Kokawa, Metall. Mater. Trans. A 32A (2001) 3023–3031.
[25] W.A. Tayon, M.S. Domack, E.K. Hoffman, S.J. Hales, Metall. Mater. Trans. A 44A (2013) 4906–4913.
[26] T. Pasang, N. Symonds, S. Moutsos, R.J.H. Wanhill, S.P. Lynch, Eng. Fail. Anal. 22 (2012) 166–178.
[27] C.G. Bennett, S.P. Lynch, R.B. Nethercott, M. Kerr, E.D. Sweet, Mater. Sci. Eng. A 247 (1998) 32–39.

[28] A.A. Csontos, E.A. Starke, Int. J. Plast. 21 (2005) 1097–1118.
[29] S.P. Lynch, Mater. Sci. Eng. A 136 (1991) 25–43.
[30] S.P. Lynch, B.C. Muddle, T. Pasang, Acta Mater. 49 (2001) 2863–2874.
[31] S.P. Lynch, A.R. Wilson, R.T. Byrnes, Mater. Sci. Eng. A 172 (1993) 79–93.
[32] K.S. Sohn, S.H. Lee, N.J. Kim, Mater. Sci. Eng. A 163 (1993) 11–21.
[33] E.D. Sweet, S.P. Lynch, C.G. Bennett, R.B. Nethercott, I. Musulin, Metall. Mater. Trans. A 27A (1996) 3530–3541.
[34] L. Zhen, Y.X. Cui, W.Z. Shao, D.Z. Yang, Mater. Sci. Eng. A 336 (2002) 135–142.
[35] D.W. Heard, J. Boselli, R. Rioja, E.A. Marquis, R. Gauvin, M. Brochu, Acta Mater. 61 (2013) 1571–1580.
[36] M.P. Seah, Acta Metall. 28 (1980) 955–962.
[37] K. Colligan, Weld. J. 78 (1999) 229S–237S.
[38] R.W. Fonda, J.F. Bingert, Metall. Mater. Trans. A 37A (2006) 3593–3604.
[39] P.A. Colegrove, H.R. Shercliff, Sci. Technol. Weld. Join. 8 (2003) 360–368.
[40] Y.S. Sato, M. Urata, H. Kokawa, Metall. Mater. Trans. A 33A (2002) 625–635.
[41] H.S. Lee, J.H. Yoon, J.T. Yoo, K. No, Friction Stir Welding Process of Aluminum-Lithium Alloy 2195, in: S. Hloch, G. Krolczyk (Eds.) International Conference on Manufacturing Engineering and Materials, Icmem 2016, pp. 62–66, 2016.
[42] M.J. Peel, A. Steuwer, P.J. Withers, T. Dickerson, Q. Shi, H. Shercliff, Metall. Mater. Trans. A 37A (2006) 2183–2193.